ACS OMEGA

http://pubs.acs.org/journal/acsodf

Article

Pyrolysis Mechanism of Wheat Straw Based on ReaxFF Molecular Dynamics Simulations

Zhiwei Liu, Xiaoke Ku,* and Hanhui Jin

Cite This: *ACS Omega* 2022, 7, 21075−21085

Read Online

ACCESS | Metrics & More | Article Recommendations

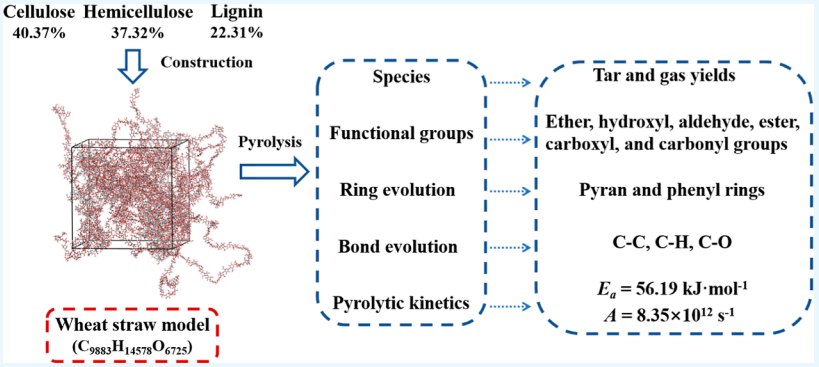

ABSTRACT: Biomass has played an increasingly important role in the consumption of energy worldwide because of its renewability and carbon-neutral property. In this work, the pyrolysis mechanism of wheat straw is explored using reactive force field molecular dynamics simulations. A large-scale wheat straw model composed of cellulose, hemicellulose, and lignin is built. After model validation, the temporal evolutions of the main pyrolysis products under different temperatures are analyzed. As the temperature rises, the gas production increases and the tar yield can decrease after peaking. Relatively high temperatures accelerate the generation rates of the main gas and tar species. CO and CO_2 molecules mainly come from the cleavage of CHO_2 radicals, and numerous H_2O molecules are generated on account of dehydration. Moreover, the evolution of six functional groups and pyran and phenyl rings as well as three types of bonds is also presented. It is observed that the phenyl rings reflect improved thermostability. Finally, the pyrolytic kinetics analysis is conducted, and the estimated activation energy of wheat straw pyrolysis is found to be 56.19 kJ/mol. All these observations can help deeply understand the pyrolytic mechanism of wheat straw biomass.

1. INTRODUCTION

Biomass, as a renewable and carbon-neutral energy source, has drawn widespread attention in recent years.[1] The utilization of biomass can not only alleviate energy shortages but also reduce environmental pollution owing to its low sulfur content.[2] Among different biomass types, lignocellulosic biomass is one of the most abundant resources, and its components include cellulose, hemicellulose, lignin, and a small amount of extractives.[3] The main thermochemical transformation processes of biomass are pyrolysis, gasification, combustion, and liquefaction.[4−6] Among these processes, pyrolysis is a promising method, during which biomass can be converted into biochar, bio-oil, biogas, or other high-quality products.[7]

To comprehend the pyrolytic behavior of biomass, numerous experimental measurements have been carried out under different conditions. Greenhalf et al.[8] and Zuo et al.[9] investigated the impact of biomass type on pyrolysis behavior. Qu et al.[10] studied the fast pyrolysis of hemicellulose, cellulose, and lignin and explored the relationship between biomass composition and pyrolytic product distribution. It was found that carbohydrates in bio-oil mainly came from cellulose, phenols were the vital part of bio-oil in lignin, and the constituents in hemicellulose bio-oil were complex. Chen et al.[11] found that the cellulose crystallinity had a positive effect on the activation energy. Ding et al.[12] compared the differences in pyrolysis behavior between hardwood and softwood and found that softwood had greater activation energy than hardwood during pyrolysis. Temperature is also a crucial factor influencing biomass pyrolysis. Xiao and Yang[13] examined the pyrolysis of rice straw in a tubular reactor. They revealed that different temperatures would affect the organic structure of semi-char and tar. Pham et al.[14] explored the phenolic compounds and aromatic hydrocarbons during

Received: March 29, 2022
Accepted: May 26, 2022
Published: June 6, 2022

https://doi.org/10.1021/acsomega.2c01899
ACS Omega 2022, 7, 21075−21085

biomass pyrolysis and claimed that their yields were affected by pyrolysis temperature. Furthermore, biochar characteristics (e.g., yield, carbon fraction, and physicochemical properties) were also susceptible to pyrolysis temperature.[15−18] Mishra and Mohanty[19] estimated the kinetic parameters of three biomass species during pyrolysis. They found that the heating rate affected the activation energy and pre-exponential factor. Besides the pyrolysis under an inert gas atmosphere, biomass oxidative pyrolysis might run without the need for an external heating system.[20,21] Sellin et al.[22] analyzed the product distribution during oxidative fast pyrolysis of banana leaves in a fluidized-bed reactor. All these experiments promoted the understanding of the biomass pyrolysis process and the effects of operating parameters such as temperature and biomass composition. However, because biomass pyrolysis is a complex process and the degradation reaction usually occurs in a short period, it still remains a huge challenge to capture all the reaction details and illuminate the pyrolysis mechanism clearly.

Due to advances in computer hardware and software, computational simulations have become an effective and powerful tool for studying the biomass pyrolysis process and exploring the fundamental reaction mechanism. Among various numerical methods, molecular dynamics (MD) using reactive force field (ReaxFF) proposed by van Duin et al.[23] has a great advantage because of its high spatiotemporal resolution, thus allowing researchers to gain insight into the complex reaction at the atomic/molecular level. Moreover, compared with the quantum mechanics (QM) methods and traditional MD methods, ReaxFF MD can simulate complex chemical reactions without predefining reaction pathways in a large molecular system. To date, ReaxFF MD has been successfully used in diverse complex systems.[24−26] For example, Beste[27] studied the oxidative process of softwood lignin and revealed the formation mechanism of formaldehyde. Zhang et al.[28,29] selected four types of lignin models to explore the reaction mechanisms of lignin pyrolysis. They found that the differences of the linkage and oxygen-containing functional groups affected the evolution of various lignin models. Li et al.[30] simulated the lignin gasification in supercritical water and uncovered the generation paths of three main gas products. Zheng et al.[31] analyzed the initial reaction mechanisms of cellulose pyrolysis and demonstrated the effectiveness of the method. Si et al.[32] investigated the effects of temperature, heating rate, and Ca/C mass ratio on cellulose pyrolysis. Chen et al.[33] constructed a simplified biomass model and simulated its pyrolysis and combustion process in oxidative and humidity environments. It was observed that more H_2 molecules were produced in a humidity atmosphere and that higher temperatures contributed to the formation of CO. However, most of these works focused on the reaction mechanism of one specific biomass component and the ReaxFF MD simulations of a real biomass species are still quite limited.

In the present work, the pyrolysis mechanism of wheat straw is probed by ReaxFF MD simulations. Specifically, a large-scale wheat straw model composed of cellulose, hemicellulose, and lignin is first built based on the ultimate analysis and components of the biomass feedstock. Afterward, the validity of the utilized method is verified by comparing the simulation results with the experimental data. Then, the temporal evolutions of the main pyrolysis products under different temperatures are analyzed. Moreover, the evolutions of six functional groups and pyran and phenyl rings as well as three types of bonds are also presented. Finally, the pyrolytic kinetics analysis is carried out and the estimated activation energy and pre-exponential factor are reported. All these results are beneficial for understanding the pyrolytic mechanism of wheat straw biomass in depth.

2. NUMERICAL METHOD

2.1. Biomass Model Construction. Excluding a small quantity of extractives, the main components of wheat straw include cellulose, hemicellulose, and lignin. The cellulose is made up of six linear chains, each of which contains 100 1,4-β-D-glucopyranose monomers.[34] The hemicellulose is highly branched and assumed to be composed of the combination of two types of arabinoxylans.[35] The lignin has the linkages of a certain number of C_9 units, which represent three types of phenylpropane skeletons mainly comprising *p*-hydroxyphenyl, guaiacyl, and syringyl units.[36−38] Here, the lignin applied consists of 11 lignin molecules, each of which has 25 C_9 units linked together.[37]

The construction of the wheat straw model is performed by using Materials Studio software. First, each molecule of the three main components is optimized by the Forcite module with the universal force field. Afterward, these molecules are packed in a cubic box with periodic boundary conditions by using the Amorphous cell module. Considering the overlap of the atoms, the initial system density is set to 0.1 g/cm^3. Second, in order to obtain an appropriate density and good geometry, the constructed model undergoes five annealing cycles of 300−700 K with the NVT ensemble. Then, the model is compressed and decompressed at pressures of 0.01 GPa and 0.1 MPa for 50 ps with the NPT ensemble, respectively. Finally, an optimized three-dimensional (3D) wheat straw model (i.e., $C_{9883}H_{14578}O_{6725}$) is obtained with a density of 0.899 g/cm^3, which is shown in Figure 1.

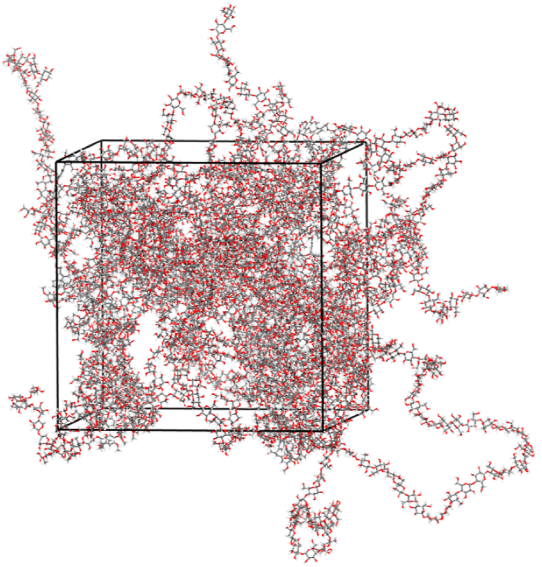

Figure 1. Optimized 3D structure of the wheat straw model (C: gray, H: white, and O: red).

In Table 1, the ultimate analyses and mass fractions of the wheat straw components used in this work are compared with the experimental results reported in the literature.[39−42] Except for the slightly higher C content and a little lower O content, the H content and three main components derived from the present model are comparable to the corresponding reported data.

https://doi.org/10.1021/acsomega.2c01899
ACS Omega 2022, 7, 21075−21085

Table 1. Ultimate Analysis and Components of Wheat Straw Used in This Work and Other Reported Works[a]

ultimate analysis (wt %)			biomass components (wt %)			
carbon	hydrogen	oxygen	cellulose	hemicellulose	lignin	sources
46.32	6.59	47.09	38.45	38.45	23.10	39
49.65	6.19	44.16	35.52	41.86	22.62	40
47.58	6.09	46.33	48.71	32.61	18.68	41
45.29	6.52	48.19	39.58	37.50	22.92	42
49.26	6.05	44.69	40.37	37.32	22.31	this work

[a]Note that the O content is obtained by difference.

These results demonstrate that the constructed wheat straw model is reasonable for conducting pyrolysis simulations.

2.2. ReaxFF MD Simulation Details. ReaxFF MD is the combination of the classical MD and the ReaxFF proposed by van Duin et al.,[23] which has become a powerful tool for simulating complex molecular systems and exploring the chemical reaction mechanisms with a high accuracy.[43,44] Different from the QM methods which normally process a small system with hundreds of atoms, ReaxFF MD can resolve the chemical reactions in large-scale molecular systems with tens of thousands of atoms. Moreover, the reaction pathways need not to be predefined because ReaxFF MD is capable of handling the chemical reactions based on the atomic distance. Similar to the classical MD, the total potential energy of a system in ReaxFF MD is calculated by eq 1.[30]

$$E_{system} = E_{bond} + E_{over} + E_{under} + E_{val} + E_{pen} + E_{tors} + E_{conj} + E_{vdWaals} + E_{Coulomb} \quad (1)$$

where the energy terms on the right-hand side of eq 1 are the bond energy term, over- and under-coordination terms, valence angle term, penalty term, torsion angle term, conjugation term, and nonbonded van der Waals and Coulomb interaction terms, respectively.

The pyrolysis simulations are carried out using the large-scale atomic/molecular massively parallel simulator (LAMMPS).[43,45] The ReaxFF parameters employed are consistent with those of Chenoweth et al.,[46] and these parameters have been proven to be applicable to many organic systems.[31,34,47−49] To economize the computational resources, a high pyrolysis temperature range of 1200−2000 K is utilized. In the reaction system, the temperature rises from the original temperature of 300 K to the target pyrolysis temperature at a heating rate of 20 K/ps. A similar choice was frequently made in the ReaxFF MD simulations.[31,50,51] The temperature is controlled by employing the Berendsen thermostat with a damping constant of 0.1 ps.[47] Moreover, the time step is 0.25 fs and a bond cutoff of 0.3 is used to identify the thermal decomposition species. A python script is developed to analyze the pyrolysis products and track the reaction events by collecting the temporal evolution of the bonds.

3. RESULTS AND DISCUSSION

3.1. Validation and Analysis of Tar and Gas Yields. To verify the numerical model, the ReaxFF MD simulation results are compared with published experimental data.[39,42] Figure 2 shows the comparison of the gas and tar mass fractions between our simulation results and the experimental data reported by Di Blasi et al.[39] Note that to accelerate the reaction and reduce the computational cost, relatively high temperatures are usually adopted in ReaxFF MD simulations.[49,50,52,53] The pyrolysis products are divided into four categories based on the number of carbon atoms, that is, gas (C_0−C_4), light tar (C_5−C_{13}), heavy tar (C_{14}−C_{40}), and char (C_{40+}).[54−56] However, several species, for example, formaldehyde (CH_2O), methanol (CH_3OH), glyoxal ($C_2H_2O_2$), acetaldehyde (CH_3CHO), and glycolaldehyde ($C_2H_4O_2$) are considered as light tar rather than gas.[57] As the temperature rises, the gas mass fraction monotonically increases, while the tar concentration first increases and then decreases. Such evolving trends are well captured by the model. In addition, Figure 3 further compares the mole fractions of four major light gases between our simulation results and the experimental data of Burhenne et al.[42] The temperatures set for the MD simulations and experiments are 2000 and 773 K, respectively. Obviously, a good agreement is obtained, indicating the strong predictive ability of the model.

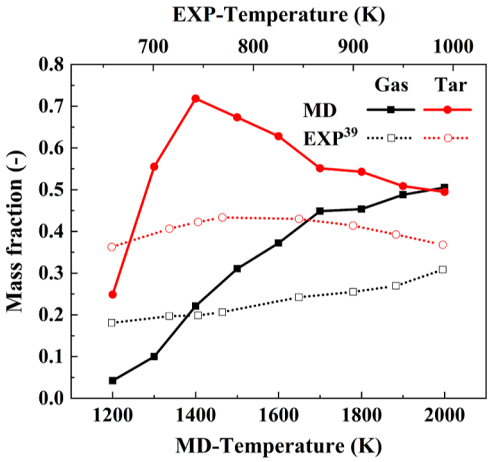

Figure 2. Comparison of the gas and tar mass fractions between the ReaxFF MD simulation and the experiment.

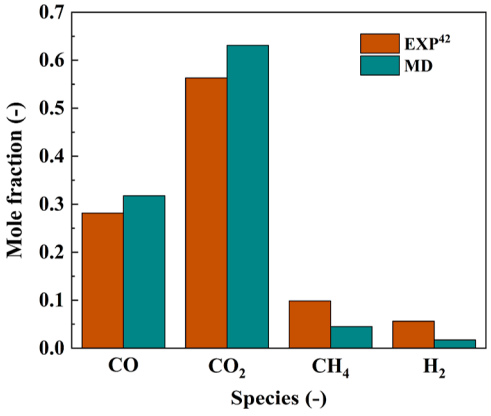

Figure 3. Comparison of the mole fractions of the major light gases between the ReaxFF simulation and the experiment.

3.2. Analysis of the Main Products. *3.2.1. Gas and Tar Yields.* Figure 4 presents the temporal evolution of the mass fractions of gas, light tar, and heavy tar at 2000 K. Note that in contrast from Figure 2, the tar is further divided into light and heavy tars in Figure 4. The yields of heavy and light tars increase rapidly at the initial stage, and heavy tar is first to be generated from thermal degradation of biomass. After reaching the peak, the productions of heavy and light tars begin to decline, although such a decrease starts earlier for the heavy tar than for the light

https://doi.org/10.1021/acsomega.2c01899
ACS Omega 2022, 7, 21075−21085

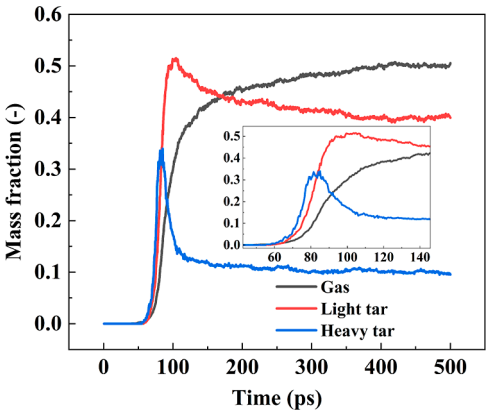

Figure 4. Temporal evolution of the mass fractions of gas, light tar, and heavy tar at 2000 K.

tar. Eventually, the yields of both heavy and light tars level off. In addition, the gas production continuously increases throughout the entire pyrolysis process. These observations reflect that the decomposition of biomass leads to the fast increase of tar and gas at the initial stage. Later, the cracking of heavy tar promotes the growth of light tar and gas. Moreover, the light tar can further decompose and also contribute to the gas yield. The above analysis demonstrates that high-carbon compounds are converted into low-carbon compounds during the pyrolysis of wheat straw.

3.2.2. Evolution of the Gas Products. Gas species with low molecular weights account for a considerable portion of the pyrolysis products. It is thus important to understand their generating mechanism and evolving behavior. Figure 5 displays the temporal evolution of the main gas products during wheat straw pyrolysis under different temperatures. The numbers of CO, CO_2, CH_4, and H_2O molecules increase gradually during pyrolysis. Increasing the temperature promotes the production of these four kinds of gas species. By analyzing the bond information, it can be found that most CO molecules form from the cleavage of some CHO_2 fragments that usually result from the ring-opening reactions of pyran rings. The CHO_2 fragments can also generate CO_2 molecules through dehydrogenation.

Meanwhile, some $C_2H_3O_2$ fragments can break into CO_2 and methyl groups during the initial stage of pyrolysis (0−100 ps). The methyl groups can further combine with hydrogen in organics to form CH_4. In addition, numerous H_2O molecules are generated on account of dehydration which probably occurs in the cellulose with many hydroxyl groups. Besides, the cellulose and hemicellulose are the primary sources to produce CO and CO_2, although slightly more CO_2 molecules come from hemicellulose owing to the potential existence of carboxyl and carbonyl groups. CH_4 is predominantly from the cellulose and lignin, although the lignin can generate more CH_4 at the same mass, probably due to plentiful methoxy groups existing in

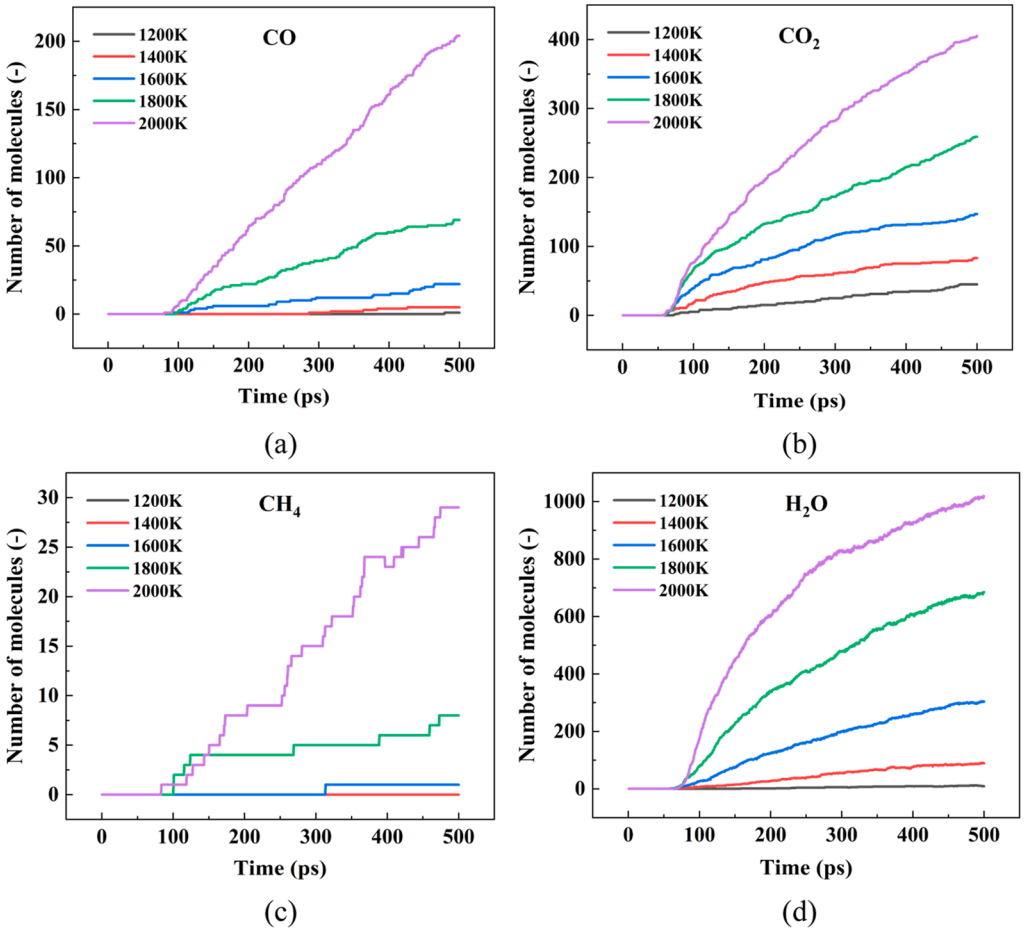

Figure 5. Temporal evolution of the main gas products during wheat straw pyrolysis under different temperatures: (a) CO, (b) CO_2, (c) CH_4, and (d) H_2O.

https://doi.org/10.1021/acsomega.2c01899
ACS Omega 2022, 7, 21075−21085

lignin. Quantitatively, Table 2 provides the percentage of each gas species resulting from the three components during the whole pyrolysis process at a temperature of 2000 K.

Table 2. Percentage (%) of Each Gas Species Resulting from the Three Components During the Whole Pyrolysis Process at 2000 K

gas	cellulose	hemicellulose	lignin
CO	48.29	44.39	7.32
CO_2	47.04	48.28	4.68
CH_4	53.33	6.67	40.00
H_2O	83.96	10.74	5.30

3.2.3. Evolution of the Tar Products. There are different kinds of tar species generated during wheat straw pyrolysis. Figure 6 presents the temporal evolution of five representative light tar products under different temperatures. It can be observed that the amount of CH_2O, CH_3OH, and CH_3CHO keeps increasing with the pyrolysis time, although the growth rate seems to diminish gradually. Moreover, increasing the temperature promotes the generation of these three kinds of tar species. When the temperature is below 2000 K, the evolving trends of $C_2H_4O_2$ and $C_2H_2O_2$ are similar to those of CH_2O, CH_3OH, and CH_3CHO. However, at 2000 K, peaks appear in the $C_2H_4O_2$ and $C_2H_2O_2$ curves. After reaching the peaks, the amount of $C_2H_4O_2$ and $C_2H_2O_2$ begins to decline.

In addition, Table 3 summarizes the percentage of each light tar species resulting from the three components during the whole pyrolysis process at a temperature of 2000 K. A close analysis of the bond information reveals that the cellulose and lignin decompose into many CH_2O molecules because of the isomerization of keto alcohol,

which further breaks down into small-molecular weight fragments at high temperatures. Due to the high oxygen content, the cellulose and hemicellulose are the main sources of $C_2H_2O_2$ and CH_3CHO. Most $C_2H_4O_2$ molecules are from the degeneration of the cellulose. In addition, CH_3OH mostly comes from the cellulose owing to the cleavage of pyran rings with rich hydroxy groups. The separation of $-OCH_3$ radicals in the lignin also supplies the precursors for the generation of CH_3OH.

3.3. Evolution of the Functional Groups and Rings. Functional groups play an important role in the pyrolysis process, which determine the chemical properties of organic compounds. Cellulose, hemicellulose, and lignin in wheat straw have different kinds and quantities of functional groups that result in their dissimilar characteristics. In addition, phenyl rings in lignin and pyran rings in cellulose and hemicellulose also have a potential effect on the thermostability of organics. Thus, the research on their evolving behaviors is beneficial to understand the mechanism of wheat straw pyrolysis.

3.3.1. Functional Groups. For the convenience of discussion here, the functional groups are classified into six primary categories: ether groups (R−O−R), hydroxyl groups (R−OH), aldehyde groups (R−CHO), ester groups (R−COO−R), carboxyl groups (R−COOH), and carbonyl groups (R−CO−R). Table 4 lists the initial numbers of these functional groups in the wheat straw model and the three components. The ether and hydroxy groups are the most abundant, while the numbers of the other four functional groups are all less than 50. The hydroxyl groups are concentrated in the cellulose and hemicellulose in the form of alcoholic hydroxyl groups.[34] The ether groups mainly come from the pyran rings and glycosidic bonds in the cellulose and hemicellulose as well as the methoxy or other carbon structures connected to the phenyl rings in the lignin.[37] The aldehyde and carbonyl groups are concentrated in the lignin, whereas the hemicellulose provides carboxyl groups. In addition, the ester groups are distributed in the hemicellulose and lignin.

Figure 7 shows the temporal evolution of the six functional groups during wheat straw pyrolysis under different temperatures. Increasing temperature usually leads to further rupture of functional groups because the unstable functional groups can break down into light gases.[13] The number of ether groups decreases as the pyrolysis progresses and higher temperatures accelerate this decrease owing to the breaking of glycosidic bonds and pyran rings.[58] A similar evolving trend is also observed for the hydroxyl groups, although a tiny increase in the number appears during the initial stage, which might be related to the breakage of the carboxyl groups. The number of the aldehyde groups continues to increase with time at low temperatures (1200−1600 K), which probably results from the fragmentation of hydroxymethyl groups and keto−enol tautomerization.[20,58] However, at high temperatures (1800−2000 K), this number begins to decrease after reaching a maximum value because the aldehydes can be further broken down. The numbers of the ester and carboxyl groups generally decrease with the pyrolysis time and temperature, although obvious fluctuations can also be discerned in the curves.

For the carbonyl groups, when the temperature is in the range of 1200−1400 K, the number variation with the time and temperature is insignificant. However, when the temperature is above 1400 K, the curves first exhibit an increase and then a decrease over time. Such a trend is more obvious at higher temperatures (e.g., 1800 and 2000 K). The appearance of the increase is because of the dehydration of hydroxyl groups in pyran rings and keto−enol tautomerization.[58,59]

3.3.2. Pyran and Phenyl Rings. There are two major kinds of rings present in the wheat straw model, that is, pyran and phenyl rings. Specifically, the cellulose and hemicellulose have pyran rings, while the lignin contains phenyl rings. Figure 8 depicts the temporal evolution of the pyran and phenyl rings during wheat straw pyrolysis under different temperatures. Both types of rings decrease with the pyrolysis time, and a higher temperature accelerates such reduction. The pyran rings are totally decomposed in 500 ps when the temperature is above 1600 K. Its rupture arises from the breaking of C−O in glucopyranose rings.[60] Compared to the pyran rings, it is harder to open the phenyl rings because of the conjugated pi bonds. Even at the highest temperature (i.e., 2000 K), the number of the broken phenyl rings is small (see Figure 8b), indicating that the phenyl rings have good thermal stability. This also reflects that the lignin is more difficult to break down than the cellulose and hemicellulose under the same processing conditions.[61]

3.4. Bond Evolution and Pyrolytic Kinetics. *3.4.1. Evolution of Bonds.* Figure 9 shows the temporal evolution of the C−C, C−H, and C−O bonds during wheat straw pyrolysis under different temperatures. Note that double bonds are statistically treated as single bonds for convenience and the bonds in benzenes are also calculated as the C−C bonds. As the pyrolysis time goes by, the numbers of all three types of bonds decrease and the decreasing rate also decreases. Moreover, higher temperatures provide more energy to accelerate the bond breaking. It can also be seen that the cleavage of the C−C and C−O bonds is concentrated in the initial stage compared to the C−H bonds.

https://doi.org/10.1021/acsomega.2c01899
ACS Omega 2022, 7, 21075−21085

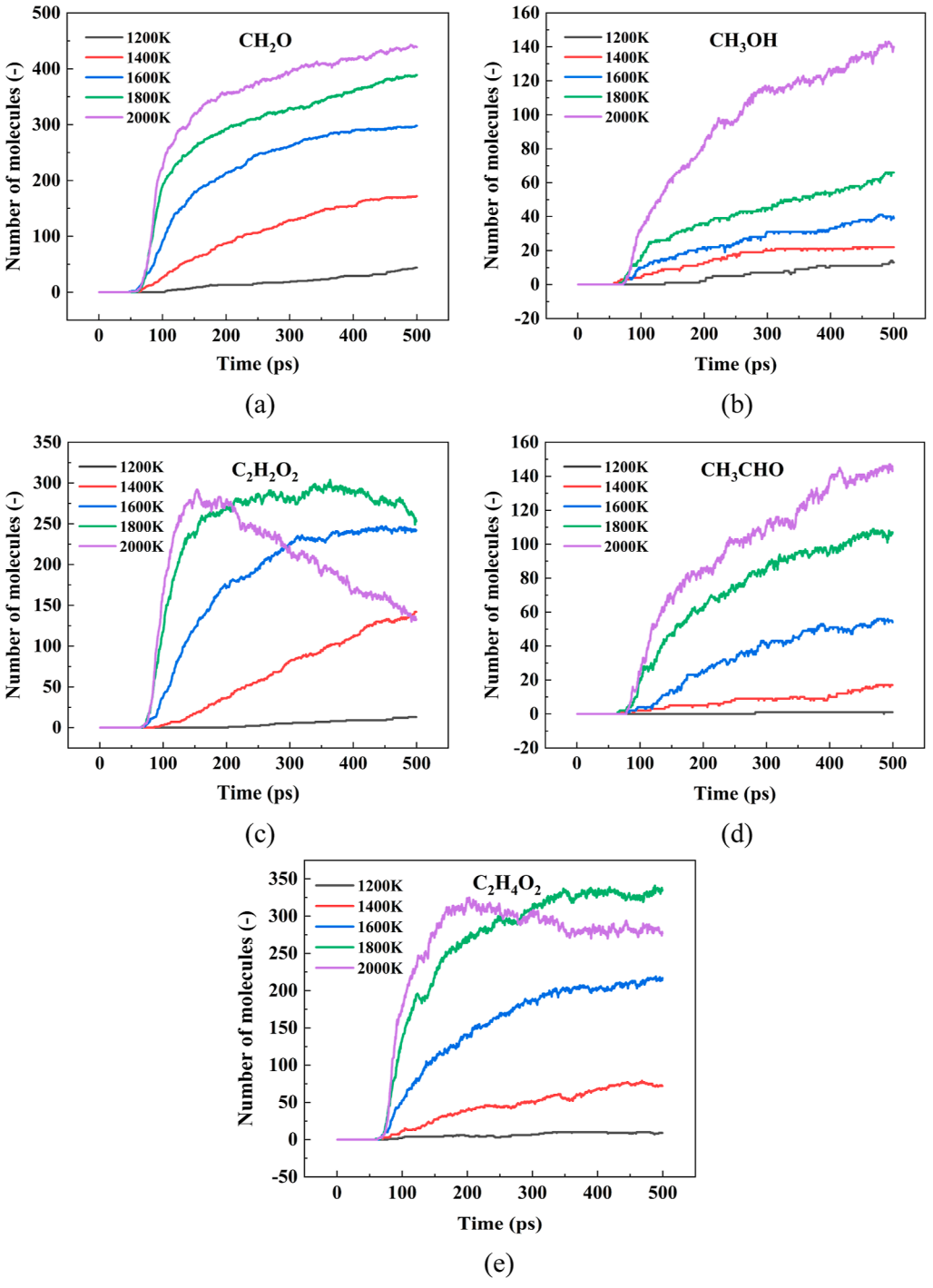

Figure 6. Temporal evolution of the tar products during wheat straw pyrolysis under different temperatures: (a) CH_2O, (b) CH_3OH, (c) $C_2H_2O_2$, (d) CH_3CHO, and (e) $C_2H_4O_2$.

Table 3. Percentage (%) of Each Light Tar Species Resulting from the Three Components During the Whole Pyrolysis Process at 2000 K

light tar	cellulose	hemicellulose	lignin
CH_2O	44.42	27.31	28.27
CH_3OH	67.55	10.60	21.85
$C_2H_2O_2$	68.19	30.34	1.47
CH_3CHO	68.71	23.01	8.28
$C_2H_4O_2$	86.47	9.11	4.42

3.4.2. Pyrolytic Kinetics. Biomass pyrolytic kinetics is routinely considered to be based on a single reaction.[7,62] Here, the time-dependent number of the C−C bonds is used to represent the degree of thermal decomposition due to its importance in organic matters.[33] Biomass decomposition is assumed to follow a first-order reaction which has been widely applied in previous works.[33,57,63−66] The rate constant can be described for each temperature by the following equation

$$\ln(1 - \alpha) = -kt \quad (2)$$

https://doi.org/10.1021/acsomega.2c01899
ACS Omega 2022, 7, 21075−21085

Table 4. Number of Functional Groups (−) in the Wheat Straw Model and Its Components

	types of functional groups					
components	ether groups	hydroxyl groups	aldehyde groups	ester groups	carboxyl groups	carbonyl groups
cellulose	1194	1806				
hemicellulose	1308	1274		34	26	
lignin	638	275	44	11		44
total	3140	3355	44	45	26	44

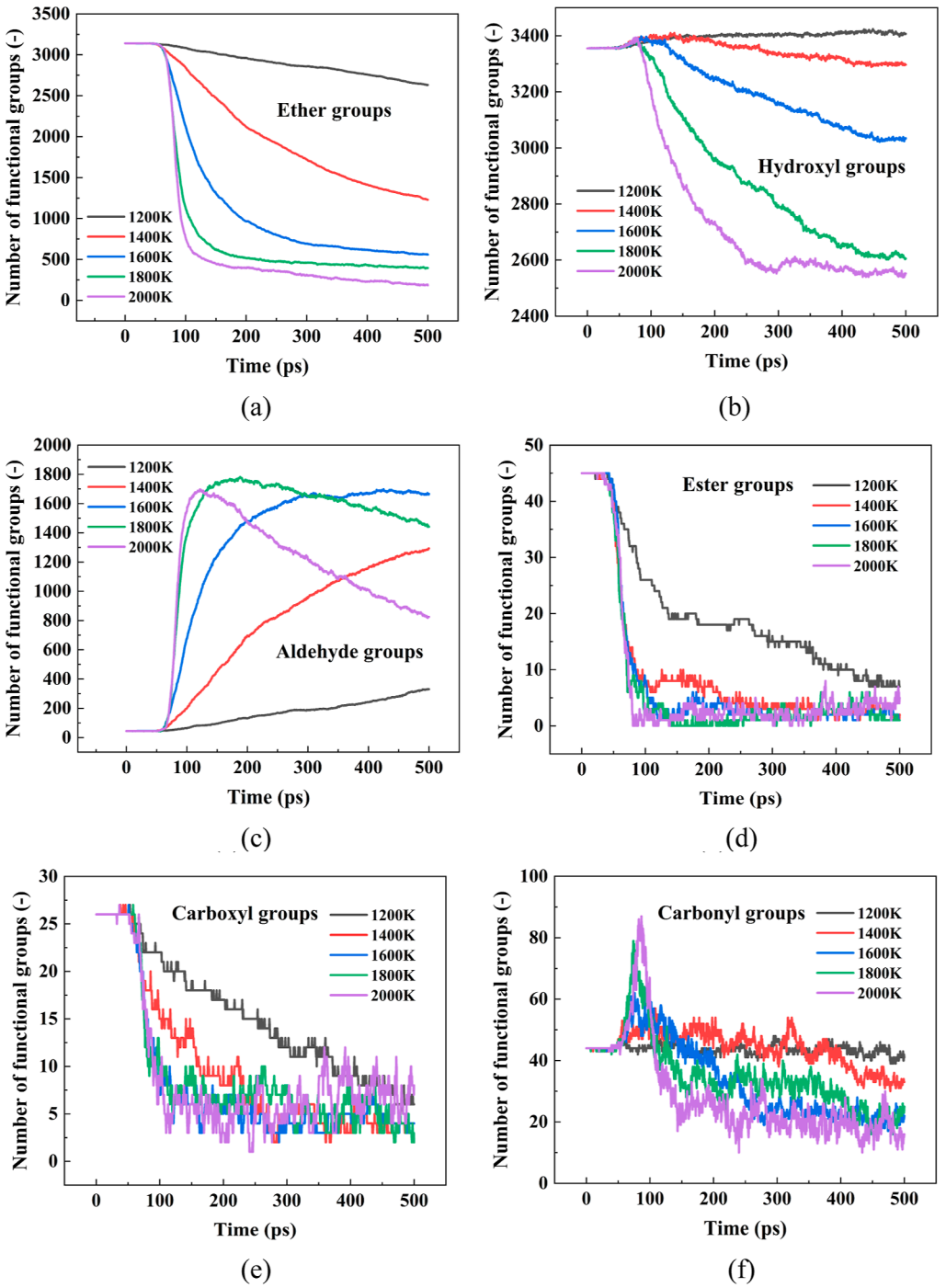

Figure 7. Temporal evolution of the functional groups during wheat straw pyrolysis under different temperatures: (a) ether, (b) hydroxyl, (c) aldehyde, (d) ester, (e) carboxyl, and (f) carbonyl groups.

where k is the rate constant. α represents the degree of the reaction at any time t and can be defined as the fraction of the cleavage of C−C bonds. The term α can be obtained as follows

$$\alpha = \frac{N_0 - N_t}{N_0 - N_f} \quad (3)$$

https://doi.org/10.1021/acsomega.2c01899
ACS Omega 2022, 7, 21075−21085

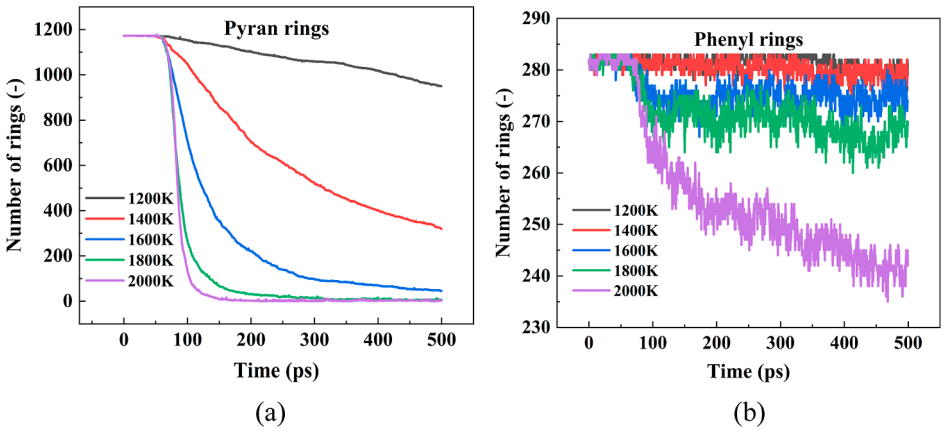

Figure 8. Temporal evolution of the (a) pyran and (b) phenyl rings during wheat straw pyrolysis under different temperatures.

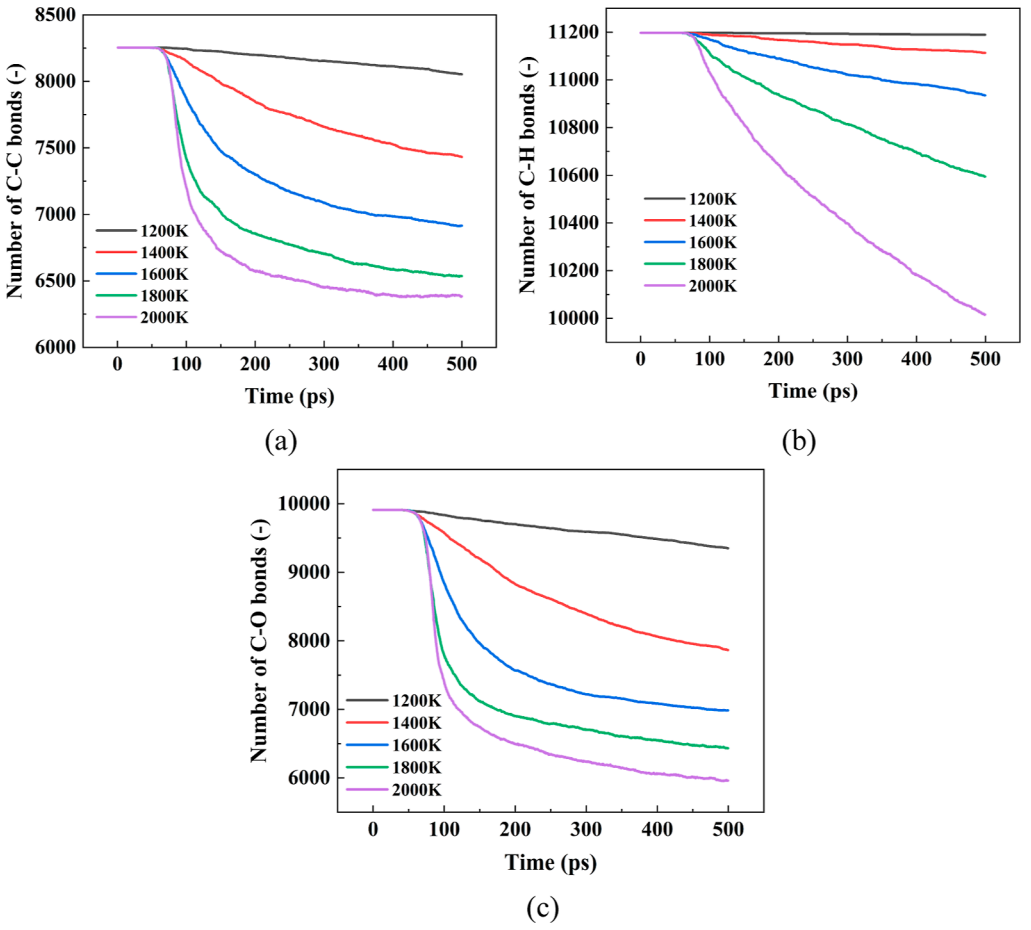

Figure 9. Temporal evolution of the (a) C−C, (b) C−H, and (c) C−O bonds during wheat straw pyrolysis under different temperatures.

where N_0, N_t, and N_f are the initial, instantaneous, and final numbers of the C−C bonds, respectively. The relevant data for α between 0.1 and 0.6 are utilized to calculate k in the temperature range of 1200−2000 K. The Arrhenius equation is given by

$$k = A \exp\left(-\frac{E_a}{RT}\right) \quad (4)$$

where A is the pre-exponential factor, E_a is the activation energy, and R is the universal gas constant. The values of A and E_a can be obtained by applying linear fitting to the Arrhenius equation on a logarithmic scale.

Figure 10 presents the relationship between the logarithm of the k and the inverse of the temperature during wheat straw pyrolysis. It is observed that the first-order kinetics data fit well with the Arrhenius equation, thus demonstrating the validity of the methodology. The predicted E_a value is 56.19 kJ/mol, which lies within the range of 31.51−74.10 kJ/mol reported in the previous experimental works.[67,68]

4. CONCLUSIONS

The pyrolysis mechanism of wheat straw is explored herein through ReaxFF MD simulations. A large-scale wheat straw model composed of cellulose, hemicellulose, and lignin is first

https://doi.org/10.1021/acsomega.2c01899
ACS Omega 2022, 7, 21075−21085

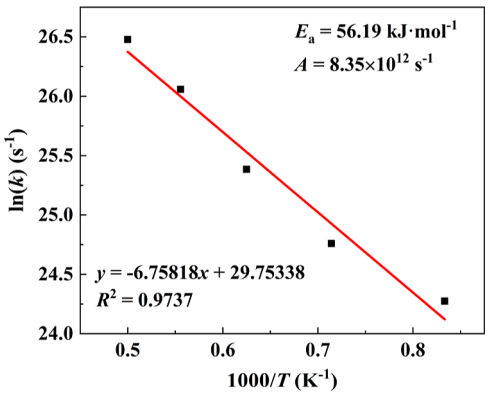

Figure 10. Relationship between the logarithm of the reaction rate and the inverse of the temperature during wheat straw pyrolysis.

built. After model validation, the temporal evolutions of the main pyrolysis products within the temperature range of 1200−2000 K are analyzed.

The maximum tar mass fraction occurs at 1400 K, while the gas yield continuously grows with the temperature; relatively high temperatures accelerate the growth rates. The generation of CO_2 is mainly from the cracking of CHO_2 radicals, and CO is also generated from the cleavage of a small number of CHO_2 radicals. CH_4 is dominantly sourced from the combination of CH_3 radicals and hydrogen atoms. Increasing the temperature improves the generation rates of representative tar species, but high temperatures will lead to decreased $C_2H_2O_2$ and $C_2H_4O_2$ contents following their peaks. Furthermore, the ether, ester, and carboxyl groups eventually decline during pyrolysis, while the hydroxyl and carbonyl groups first climb up and then decline. The aldehyde groups continue to increase at low temperatures and decrease at high temperatures after reaching peaks. In addition, the pyrolytic kinetics analysis is conducted, and the estimated activation energy and pre-exponential factor of wheat straw pyrolysis are reported. All these observations can help us understand the pyrolytic mechanism of wheat straw biomass in depth.

AUTHOR INFORMATION

Corresponding Author

Xiaoke Ku − *Department of Engineering Mechanics and State Key Laboratory of Clean Energy Utilization, Zhejiang University, 310027 Hangzhou, China;* orcid.org/0000-0002-2182-3933; Phone: +8657187952221; Email: xiaokeku@zju.edu.cn

Authors

Zhiwei Liu − *Department of Engineering Mechanics, Zhejiang University, 310027 Hangzhou, China*

Hanhui Jin − *Department of Engineering Mechanics, Zhejiang University, 310027 Hangzhou, China*

Complete contact information is available at: https://pubs.acs.org/10.1021/acsomega.2c01899

Notes

The authors declare no competing financial interest.

ACKNOWLEDGMENTS

This work was financially supported by the National Natural Science Foundation of China (project numbers 51876191 and 12172328), the Zhejiang Provincial Natural Science Foundation of China (project number LXR22A020001), and the Fundamental Research Funds for the Central Universities (project number 2021FZZX001-11).

REFERENCES

(1) Vassilev, S. V.; Vassileva, C. G.; Vassilev, V. S. Advantages and Disadvantages of Composition and Properties of Biomass in Comparison with Coal: An Overview. *Fuel* **2015**, *158*, 330−350.

(2) Turconi, R.; Boldrin, A.; Astrup, T. Life Cycle Assessment (LCA) of Electricity Generation Technologies: Overview, Comparability and Limitations. *Renewable Sustainable Energy Rev.* **2013**, *28*, 555−565.

(3) Cai, J.; He, Y.; Yu, X.; Banks, S. W.; Yang, Y.; Zhang, X.; Yu, Y.; Liu, R.; Bridgwater, A. V. Review of Physicochemical Properties and Analytical Characterization of Lignocellulosic Biomass. *Renewable Sustainable Energy Rev.* **2017**, *76*, 309−322.

(4) Goyal, H. B.; Seal, D.; Saxena, R. C. Bio-Fuels from Thermochemical Conversion of Renewable Resources: A Review. *Renewable Sustainable Energy Rev.* **2008**, *12*, 504−517.

(5) Fatehi, H.; Weng, W.; Li, Z.; Bai, X.-S.; Aldén, M. Recent Development in Numerical Simulations and Experimental Studies of Biomass Thermochemical Conversion. *Energy Fuels* **2021**, *35*, 6940−6963.

(6) Seo, M. W.; Lee, S. H.; Nam, H.; Lee, D.; Tokmurzin, D.; Wang, S.; Park, Y.-K. Recent Advances of Thermochemical Conversieon Processes for Biorefinery. *Bioresour. Technol.* **2022**, *343*, 126109.

(7) Hu, B.; Gu, Z.; Su, J.; Li, Z. Pyrolytic Characteristics and Kinetics of Guanzhong Wheat Straw and Its Components for High-Value Products. *Bioresources* **2021**, *16*, 1958−1979.

(8) Greenhalf, C. E.; Nowakowski, D. J.; Harms, A. B.; Titiloye, J. O.; Bridgwater, A. V. A Comparative Study of Straw, Perennial Grasses and Hardwoods in Terms of Fast Pyrolysis Products. *Fuel* **2013**, *108*, 216−230.

(9) Zuo, Z.; Yu, Q.; Xie, H.; Duan, W.; Liu, S.; Qin, Q. Thermogravimetric Analysis of the Biomass Pyrolysis with Copper Slag as Heat Carrier: Pyrolysis Characteristics and Kinetics. *J. Therm. Anal. Calorim.* **2017**, *129*, 1233−1241.

(10) Qu, T.; Guo, W.; Shen, L.; Xiao, J.; Zhao, K. Experimental Study of Biomass Pyrolysis Based on Three Major Components: Hemicellulose, Cellulose, and Lignin. *Ind. Eng. Chem. Res.* **2011**, *50*, 10424−10433.

(11) Chen, H.; Liu, Z.; Chen, X.; Chen, Y.; Dong, Z.; Wang, X.; Yang, H. Comparative Pyrolysis Behaviors of Stalk, Wood and Shell Biomass: Correlation of Cellulose Crystallinity and Reaction Kinetics. *Bioresour. Technol.* **2020**, *310*, 123498.

(12) Ding, Y.; Ezekoye, O. A.; Lu, S.; Wang, C.; Zhou, R. Comparative Pyrolysis Behaviors and Reaction Mechanisms of Hardwood and Softwood. *Energy Convers. Manage.* **2017**, *132*, 102−109.

(13) Xiao, R.; Yang, W. Influence of Temperature on Organic Structure of Biomass Pyrolysis Products. Renew. *Energy* **2013**, *50*, 136−141.

(14) Hoang Pham, L. K.; Vi Tran, T. T.; Kongparakul, S.; Reubroycharoen, P.; Ding, M.; Guan, G.; Vo, D.-V. N.; Jaiyong, P.; Youngvises, N.; Samart, C. Data-Driven Prediction of Biomass Pyrolysis Pathways toward Phenolic and Aromatic Products. *J. Environ. Chem. Eng.* **2021**, *9*, 104836.

(15) Wei, S.; Zhu, M.; Fan, X.; Song, J.; Peng, P. a.; Li, K.; Jia, W.; Song, H. Influence of Pyrolysis Temperature and Feedstock on Carbon Fractions of Biochar Produced from Pyrolysis of Rice Straw, Pine Wood, Pig Manure and Sewage Sludge. *Chemosphere* **2019**, *218*, 624−631.

(16) Ortiz, L. R.; Torres, E.; Zalazar, D.; Zhang, H.; Rodriguez, R.; Mazza, G. Influence of Pyrolysis Temperature and Bio-Waste Composition on Biochar Characteristics. *Renewable Energy* **2020**, *155*, 837−847.

(17) Rodriguez, J. A.; Filho, J. F. L.; Melo, L. C. A.; de Assis, I. R.; de Oliveira, T. S. Influence of Pyrolysis Temperature and Feedstock on the Properties of Biochars Produced from Agricultural and Industrial Wastes. *J. Anal. Appl. Pyrolysis* **2020**, *149*, 104839.

(18) Kim, K. H.; Kim, J.-Y.; Cho, T.-S.; Choi, J. W. Influence of Pyrolysis Temperature on Physicochemical Properties of Biochar Obtained from the Fast Pyrolysis of Pitch Pine (Pinus Rigida). *Bioresour. Technol.* **2012**, *118*, 158−162.
(19) Mishra, R. K.; Mohanty, K. Pyrolysis Characteristics and Kinetic Parameters Assessment of Three Waste Biomass. *J. Renew. Sustain. Energy* **2018**, *10*, 013102.
(20) Zhao, S.; Bi, X.; Sun, R.; Niu, M.; Pan, X. Density Functional Theory and Experimental Study of Cellulose Initial Degradation Stage under Inert and Oxidative Atmosphere. *J. Mol. Struct.* **2020**, *1204*, 127543.
(21) Ma, C.; Sánchez-Rodríguez, D.; Kamo, T. A Comprehensive Study on the Oxidative Pyrolysis of Epoxy Resin from Fiber/Epoxy Composites: Product Characteristics and Kinetics. *J. Hazard. Mater.* **2021**, *412*, 125329.
(22) Sellin, N.; Krohl, D. R.; Marangoni, C.; Souza, O. Oxidative Fast Pyrolysis of Banana Leaves in Fluidized Bed Reactor. *Renewable Energy* **2016**, *96*, 56−64.
(23) van Duin, A. C. T.; Dasgupta, S.; Lorant, F.; Goddard, W. A. ReaxFF: A Reactive Force Field for Hydrocarbons. *J. Phys. Chem. A* **2001**, *105*, 9396−9409.
(24) Castro-Marcano, F.; van Duin, A. C. T. Comparison of Thermal and Catalytic Cracking of 1-Heptene from ReaxFF Reactive Molecular Dynamics Simulations. *Combust. Flame* **2013**, *160*, 766−775.
(25) Gao, M.; Li, X.; Guo, L. Pyrolysis Simulations of Fugu Coal by Large-Scale ReaxFF Molecular Dynamics. *Fuel Process. Technol.* **2018**, *178*, 197−205.
(26) Kwon, H.; Shabnam, S.; van Duin, A. C. T.; Xuan, Y. Numerical Simulations of Yield-Based Sooting Tendencies of Aromatic Fuels Using ReaxFF Molecular Dynamics. *Fuel* **2020**, *262*, 116545.
(27) Beste, A. ReaxFF Study of the Oxidation of Lignin Model Compounds for the Most Common Linkages in Softwood in View of Carbon Fiber Production. *J. Phys. Chem. A* **2014**, *118*, 803−814.
(28) Zhang, T.; Li, X.; Qiao, X.; Zheng, M.; Guo, L.; Song, W.; Lin, W. Initial Mechanisms for an Overall Behavior of Lignin Pyrolysis through Large-Scale ReaxFF Molecular Dynamics Simulations. *Energy Fuels* **2016**, *30*, 3140−3150.
(29) Zhang, T.; Li, X.; Guo, L.; Guo, X. Reaction Mechanisms in Pyrolysis of Hardwood, Softwood, and Kraft Lignin Revealed by ReaxFF MD Simulations. *Energy Fuels* **2019**, *33*, 11210−11225.
(30) Li, H.; Xu, B.; Jin, H.; Luo, K.; Fan, J. Molecular Dynamics Investigation on the Lignin Gasification in Supercritical Water. *Fuel Process. Technol.* **2019**, *192*, 203−209.
(31) Zheng, M.; Wang, Z.; Li, X.; Qiao, X.; Song, W.; Guo, L. Initial Reaction Mechanisms of Cellulose Pyrolysis Revealed by ReaxFF Molecular Dynamics. *Fuel* **2016**, *177*, 130−141.
(32) Si, T.; Huang, K.; Lin, Y.; Gu, M. ReaxFF Study on the Effect of CaO on Cellulose Pyrolysis. *Energy Fuels* **2019**, *33*, 11067−11077.
(33) Chen, C.; Zhao, L.; Wang, J.; Lin, S. Reactive Molecular Dynamics Simulations of Biomass Pyrolysis and Combustion under Various Oxidative and Humidity Environments. *Ind. Eng. Chem. Res.* **2017**, *56*, 12276−12288.
(34) Liu, Z.; Ku, X.; Jin, H.; Yang, S. Research on the Microscopic Reaction Mechanism of Cellulose Pyrolysis Using the Molecular Dynamics Simulation. *J. Anal. Appl. Pyrolysis* **2021**, *159*, 105333.
(35) Puls, J. Chemistry and Biochemistry of Hemicelluloses: Relationship between Hemicellulose Structure and Enzymes Required for Hydrolysis. *Macromol. Symp.* **1997**, *120*, 183−196.
(36) Freudenberg, K. Biosynthesis and Constitution of Lignin. *Nature* **1959**, *183*, 1152−1155.
(37) Nimz, H. Beech Lignin—Proposal of a Constitutional Scheme. *Angew. Chem., Int. Ed.* **1974**, *13*, 313−321.
(38) Ralph, J.; Lapierre, C.; Boerjan, W. Lignin Structure and Its Engineering. *Curr. Opin. Biotechnol.* **2019**, *56*, 240−249.
(39) Di Blasi, C.; Signorelli, G.; Di Russo, C.; Rea, G. Product Distribution from Pyrolysis of Wood and Agricultural Residues. *Ind. Eng. Chem. Res.* **1999**, *38*, 2216−2224.
(40) Farooq, M. Z.; Zeeshan, M.; Iqbal, S.; Ahmed, N.; Shah, S. A. Y. Influence of Waste Tire Addition on Wheat Straw Pyrolysis Yield and Oil Quality. *Energy* **2018**, *144*, 200−206.
(41) Lazdovica, K.; Liepina, L.; Kampars, V. Comparative Wheat Straw Catalytic Pyrolysis in the Presence of Zeolites, Pt/C, and Pd/C by Using TGA-FTIR Method. *Fuel Process. Technol.* **2015**, *138*, 645−653.
(42) Burhenne, L.; Messmer, J.; Aicher, T.; Laborie, M.-P. The Effect of the Biomass Components Lignin, Cellulose and Hemicellulose on TGA and Fixed Bed Pyrolysis. *J. Anal. Appl. Pyrolysis* **2013**, *101*, 177−184.
(43) Aktulga, H. M.; Fogarty, J. C.; Pandit, S. A.; Grama, A. Y. Parallel Reactive Molecular Dynamics: Numerical Methods and Algorithmic Techniques. *Angew. Chem., Int. Ed.* **2012**, *38*, 245−259.
(44) Srinivasan, S. G.; Van Duin, A. C. T.; Ganesh, P. Development of a ReaxFF Potential for Carbon Condensed Phases and Its Application to the Thermal Fragmentation of a Large Fullerene. *J. Phys. Chem. A* **2015**, *119*, 571−580.
(45) Thompson, A. P.; Aktulga, H. M.; Berger, R.; Bolintineanu, D. S.; Brown, W. M.; Crozier, P. S.; Kohlmeyer, A.; Moore, S. G.; Nguyen, T. D.; Shan, R.; Stevens, M. J.; Tranchida, J.; Trott, C.; Plimpton, S. J. LAMMPS - a Flexible Simulation Tool for Particle-Based Materials Modeling at the Atomic, Meso, and Continuum Scales. *Comput. Phys. Commun.* **2022**, *271*, 108171.
(46) Chenoweth, K.; van Duin, A. C. T.; Goddard, W. A. ReaxFF Reactive Force Field for Molecular Dynamics Simulations of Hydrocarbon Oxidation. *J. Phys. Chem. A* **2008**, *112*, 1040−1053.
(47) Cheng, X.-M.; Wang, Q.-D.; Li, J.-Q.; Wang, J.-B.; Li, X.-Y. ReaxFF Molecular Dynamics Simulations of Oxidation of Toluene at High Temperatures. *J. Phys. Chem. A* **2012**, *116*, 9811−9818.
(48) Liu, L.; Chen, S.; Xu, H.; Zhu, Q.; Ren, H. Effect of Alkyl Substituent for Cyclohexane on Pyrolysis towards Sooting Tendency from Theoretical Principle. *J. Anal. Appl. Pyrolysis* **2022**, *161*, 105386.
(49) Salmon, E.; van Duin, A. C. T.; Lorant, F.; Marquaire, P.-M.; Goddard, W. A. Thermal Decomposition Process in Algaenan of Botryococcus Braunii Race L. Part 2: Molecular Dynamics Simulations Using the ReaxFF Reactive Force Field. *Org. Geochem.* **2009**, *40*, 416−427.
(50) Xu, F.; Liu, H.; Wang, Q.; Pan, S.; Zhao, D.; Liu, Q.; Liu, Y. ReaxFF-Based Molecular Dynamics Simulation of the Initial Pyrolysis Mechanism of Lignite. *Fuel Process. Technol.* **2019**, *195*, 106147.
(51) Liu, Q.; Liu, S.; Lv, Y.; Hu, P.; Huang, Y.; Kong, M.; Li, G. Atomic-Scale Insight into the Pyrolysis of Polycarbonate by ReaxFF-Based Reactive Molecular Dynamics Simulation. *Fuel* **2020**, *287*, 119484.
(52) Jin, H.; Xu, B.; Li, H.; Ku, X.; Fan, J. Numerical Investigation of Coal Gasification in Supercritical Water with the ReaxFF Molecular Dynamics Method. *Int. J. Hydrogen Energy* **2018**, *43*, 20513−20524.
(53) Li, X.; Zheng, M.; Ren, C.; Guo, L. ReaxFF Molecular Dynamics Simulations of Thermal Reactivity of Various Fuels in Pyrolysis and Combustion. *Energy Fuels* **2021**, *35*, 11707−11739.
(54) Xu, F.; Liu, H.; Wang, Q.; Pan, S.; Zhao, D.; Liu, Y. Study of Non-Isothermal Pyrolysis Mechanism of Lignite Using ReaxFF Molecular Dynamics Simulations. *Fuel* **2019**, *256*, 115884.
(55) Li, G.-Y.; Ding, J.-X.; Zhang, H.; Hou, C.-X.; Wang, F.; Li, Y.-Y.; Liang, Y.-H. ReaxFF Simulations of Hydrothermal Treatment of Lignite and Its Impact on Chemical Structures. *Fuel* **2015**, *154*, 243−251.
(56) Zheng, M.; Li, X.; Liu, J.; Guo, L. Initial Chemical Reaction Simulation of Coal Pyrolysis via ReaxFF Molecular Dynamics. *Energy Fuels* **2013**, *27*, 2942−2951.
(57) Chen, T.; Ku, X.; Li, T.; Karlsson, B. S. A.; Sjöblom, J.; Ström, H. High-Temperature Pyrolysis Modeling of a Thermally Thick Biomass Particle Based on an MD-Derived Tar Cracking Model. *Chem. Eng. J.* **2021**, *417*, 127923.
(58) Yang, H.; Gong, M.; Hu, J.; Liu, B.; Chen, Y.; Xiao, J.; Li, S.; Dong, Z.; Chen, H. Cellulose Pyrolysis Mechanism Based on Functional Group Evolutions by Two-Dimensional Perturbation Correlation Infrared Spectroscopy. *Energy Fuels* **2020**, *34*, 3412−3421.

https://doi.org/10.1021/acsomega.2c01899
ACS Omega 2022, 7, 21075−21085

(59) Yang, H.; Li, S.; Liu, B.; Chen, Y.; Xiao, J.; Dong, Z.; Gong, M.; Chen, H. Hemicellulose Pyrolysis Mechanism Based on Functional Group Evolutions by Two-Dimensional Perturbation Correlation Infrared Spectroscopy. *Fuel* **2020**, *267*, 117302.
(60) Dai, G.; Wang, K.; Wang, G.; Wang, S. Initial Pyrolysis Mechanism of Cellulose Revealed by In-Situ DRIFT Analysis and Theoretical Calculation. *Combust. Flame* **2019**, *208*, 273−280.
(61) Yang, H.; Dong, Z.; Liu, B.; Chen, Y.; Gong, M.; Li, S.; Chen, H. A New Insight of Lignin Pyrolysis Mechanism Based on Functional Group Evolutions of Solid Char. *Fuel* **2021**, *288*, 119719.
(62) White, J. E.; Catallo, W. J.; Legendre, B. L. Biomass Pyrolysis Kinetics: A Comparative Critical Review with Relevant Agricultural Residue Case Studies. *J. Anal. Appl. Pyrolysis* **2011**, *91*, 1−33.
(63) Wang, Q.-D.; Wang, J.-B.; Li, J.-Q.; Tan, N.-X.; Li, X.-Y. Reactive Molecular Dynamics Simulation and Chemical Kinetic Modeling of Pyrolysis and Combustion of N-Dodecane. *Combust. Flame* **2011**, *158*, 217−226.
(64) Zhang, J.; Gu, J.; Han, Y.; Li, W.; Gan, Z.; Gu, J. Supercritical Water Oxidation vs Supercritical Water Gasification: Which Process Is Better for Explosive Wastewater Treatment? *Ind. Eng. Chem. Res.* **2015**, *54*, 1251−1260.
(65) Kwon, H.; Lele, A.; Zhu, J.; McEnally, C. S.; Pfefferle, L. D.; Xuan, Y.; van Duin, A. C. T. ReaxFF-Based Molecular Dynamics Study of Bio-Derived Polycyclic Alkanes as Potential Alternative Jet Fuels. *Fuel* **2020**, *279*, 118548.
(66) Wen, Y.; Xie, Y.; Jiang, C.; Li, W.; Hou, Y. Products Distribution and Interaction Mechanism during Co-Pyrolysis of Rice Husk and Oily Sludge by Experiments and Reaction Force Field Simulation. *Bioresour. Technol.* **2021**, *329*, 124822.
(67) Lanzetta, M.; Di Blasi, C. Pyrolysis Kinetics of Wheat and Corn Straw. *J. Anal. Appl. Pyrolysis* **1998**, *44*, 181−192.
(68) Shuangning, X.; Weiming, Y.; Li, B. Flash Pyrolysis of Agricultural Residues Using a Plasma Heated Laminar Entrained Flow Reactor. *Biomass Bioenergy* **2005**, *29*, 135−141.

https://doi.org/10.1021/acsomega.2c01899
ACS Omega 2022, 7, 21075−21085